Conference paper

Silicon-germanium heterostructures: properties, technology, and application in infrared detectors+

M. A. HERMAN*

Institute of Vacuum Technology and Institute of Physics,
Polish Academy of Sciences, Warsaw

The structural and optoelectronic properties, as well as epitaxial growth peculiarities of thin film strained layer $Si_{1-x}Ge_x/Si$ heterostructures are described, highlighting the potentials of these multilayer structures to application in infrared detectors. The 4.17% lattice mismatch between Si and Ge is the reason for considering the Si-based heteroepitaxy realized with the $Si_{1-x}Ge_x$ alloy as strained layer epitaxy. Consequently, the effects of strain on epitaxial growth and on optoelectronic properties of $Si_{1-x}Ge_x/Si$ heterostructures are described and discussed in this paper, too. As examples of application of silicon-germanium heterostructures in infrared detectors only the most interesting types of detector structures are considered. These are: p-i-n photodiodes, detectors based on intersubband absorption effects, and internal photoemission detectors. The paper is concluded with a short estimation of the impact which $Si_{1-x}Ge_x/Si$ heterostructures could have on future infrared optoelectronics, with emphasis put on infrared photodetectors.

1. Introduction

The interest in $Si_{1-x}Ge_x$ alloys dates back to the year 1939, when the first homogeneous alloys of SiGe have been prepared, but the use of epitaxy in Si technology was studied much later in 1963 [1]. However, it was not applied to the growth of $Si_{1-x}Ge_x/Si$ heteroepitaxial layers until about twenty years ago [2]. The main challenge in epitaxial growth of this material system is the fact that the lattice constants of Si and Ge differ by 4.17%, and hence, it is quite difficult to grow dislocation-free $Si_{1-x}Ge_x$ layers on Si substrates. The lattice mismatch between the two materials can be, however, accommodated by a finite degree of lattice distortion (pseudomorphic strained layers), after which planar film growth (layer-by-layer growth mode) either converts to three-dimensional growth (Stranski-Krastanov growth mode), or misfit dislocations nucleate at the heterointerface, thus, relaxing the lattice strain [3]. The last two decades have seen tremendous advances towards pseudomorphic growth of $Si_{1-x}Ge_x/Si$ heterostructures [4]. Using such sophisticated techniques as molecular beam epitaxy (MBE) and ultrahigh vacuum chemical vapor deposition (UHV CVD), one can currently grow heterostructures of this material system with very low densities of defects [5].

Strain plays a dominant role in determining the alignment of energy bands at heterointerfaces, thus, determining, e.g., the confinement energy of electrons (holes) in quantum wells [1]. Strain modifies also the crystal symmetry, thus, offers the possibility of influencing the recombination rates of electrons and holes in device structures. Consequently, understanding and manipulation of strain became the natural prerequisite for device applications of $Si_{1-x}Ge_x/Si$ heterostructures.

Usually four different types of infrared detectors for the wavelength range from 1 to 18 μm are fabri-

* corresponding author: Institute of Vacuum Technology, 44/50 Długa Str., PL-00-241 Warszawa, Poland, phone: (+48) (22) 831-51-54, fax: (+48) (22) 831-21-60, e-mail:herman@alpha1.ifpan.edu.pl.

+ Presented at the 12th School of Optoelectronics: Photovoltaics – Solar Cells and Infrared Detectors, Kazimierz Dolny, May 22-24, 1997.

cated. These are: photoconductors, p-i-n photodiodes, intersubband absorption detectors, and internal photoemission detectors. All of them have been also fabricated when $Si_{1-x}Ge_x/Si$ heterostructures were used as detecting material [4]. In this paper only the last three types of detectors made of $Si_{1-x}Ge_x/Si$ heterostructures will be discussed, taking into consideration the material peculiarities of $Si_{1-x}Ge_x$ alloys.

2. $Si_{1-x-y}Ge_xC_y/Si$ heterostructures

III-V and II-VI compound semiconductors have been traditionally used in optoelectronics for many years, due to the availability of heterostructures of both, lattice matched and lattice mismatched (strained) materials in which direct band-to-band electronic transitions prevail. Introduction of $Si_{1-x}Ge_x$ or $Si_{1-x-y}Ge_xC_y$ alloys to optoelectronic device structures allows heterostructures to be fabricated in traditional Si-only technologies, which expands the potential of Si in optoelectronics [6].

A possibility of combining the low cost advantages of the Si-technology with the high performance nature of III-V or II-VI heterostructures is believed to accelerate the broad application of the above mentioned silicon-based heterostructures in optoelectronic integrated circuits, quantum well lasers, as well as in infrared photodetectors manufactured commercially.

The constituent materials of these heterostructures are composed, in general, of C, Si and Ge. The structural parameters and energy band gaps of these elements are given in Table 1.

Table 1. Structural parameters and bandgaps of the elements C, Si and Ge (after Ref. 7).

Element	Atomic Number	Crystal Lattice		Structure, bond length (Å)	Bandgap: indirect, direct (eV)
		constant (Å)	mismatch to Si (%)		
C diamond	6	3.567	–34.32	diamond 1.55	5.48 7.3
Si	14	5.431	0	diamond 2.34	1.11 3.4
Ge	32	5.657	+4.17	diamond 2.44	0.664 0.8

In silicon-based heterostructures usually one or more heterointerfaces of the form: Si/binary compound or Si/ternary compound occur. The binaries and the carbon-containing ternary compound, grown so far on Si substrates, are listed in Table 2.

Table 2. Binary solid compounds and the carbon-containing ternary compound of silicon-based heterostructures (after Ref. 8).

Alloy	Composition of epilayers	Growth techniques
$Si_{1-x}Ge_x$	$0 \le x \le 1$	GS MBE SS MBE
$Si_{1-x}C_x$	$x \le 0.02$	SS MBE interdiffusion in C delta-doped Si structure
$Ge_{1-x}C_x$	$x \le 0.4$	SS MBE with Sb as surfactant
$Si_{1-x-y}Ge_xC_y$	$y \le 0.02$ $x = 8.2y$ leads to lattice match with Si	SS MBE

For many applications of lattice mismatched materials creating heterostructures the use of Vegard's law is practical. This law expresses the linear interpolation of the lattice constant of alloys in dependence on parameter (or parameters) defining the chemical composition of the alloy (compound). For the binary compound $Si_{1-x}Ge_x$ Vegard's law has the form of

$$a_o(x) = a_{Si}(1 - x) + a_{Ge}x \qquad (1)$$

where $a_o(x)$ is the lattice constant of $Si_{1-x}Ge_x$. However, frequently a deviation from Vegard's law has to be considered for more exact analysis [9]. A systematic investigation of $Si_{1-x}Ge_x$ thin film lattice properties as a function of the Ge content confirmed a slight negative deviation of the alloy's lattice constant from Vegard's law. The following quadratic approximation formula has been recommended [9]

$$\Delta = a_o(x) - a_{Si}(1 - x) - a_{Ge}x = 2.733\ x\ (1 - x) \qquad (2)$$

where the lattice constants are expressed in picometers (pm). This deviation, Δ, amounts up to a maximum of

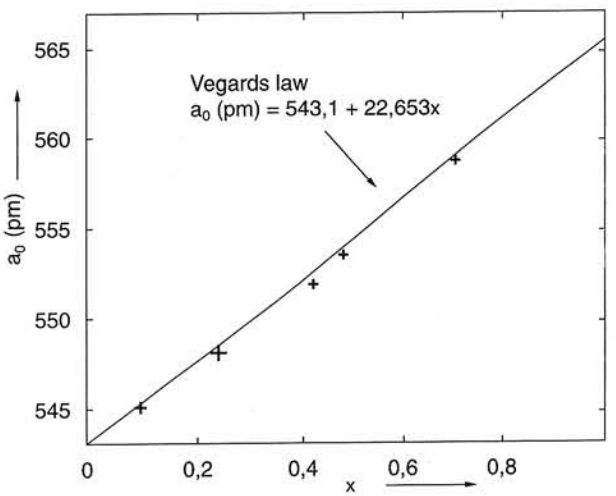

Fig. 1. Lattice constant $a_o(x)$ of $Si_{1-x}Ge_x$ layers versus Ge content x (taken from Ref.9).

the equivalent of 3% Ge content difference. The results of lattice constant $a_o(x)$ versus Ge content (x) measurements are presented in Fig. 1 and compared with the linear relationship (Vegard's law). For this relationship the lattice constants a_{Si} = 543,10 pm and a_{Ge} = 565,75 pm were assumed.

It is well known [10], that strain in pseudomorphic $Si_{1-x}Ge_x$ epilayers grown by MBE on Si(001) substrates can be adjusted by adding small amounts of carbon to the growing epilayers. A strain-free $Si_{1-x-y}Ge_xC_y$ epilayer can be grown on this substrate by choosing the concentrations x and y such that the volume changes due to the Ge and C atoms will compensate in the ternary alloy. Using simple linear extrapolations between the lattice constants in SiC, Si and Ge [6] and the appropriate relative concentrations (Vegard's law for a ternary system) one is able to estimate the effective structure in the $Si_{1-x-y}Ge_xC_y$ system grown on Si(001) as lattice matched epilayer. The relevant equation has the form

$$a_{SiGeC}(x,y) = (1 - x - y)a_{Si} + xa_{SiGe} + ya_{SiC} \quad (3)$$

and the results of such an estimation [10] are shown in Fig.2. An interesting feature in Fig.2 is the line for zero misfit. One may recognize that approximately one percent of carbon is needed to reduce the effective strain in a $Si_{0.9}Ge_{0.1}$ layer to zero. It has been shown in [10], that for a Ge/C ratio of about ten the lattice constant in growth direction is indistinguishable to that of the substrate, indicating the absence of macroscopic strain in such structure.

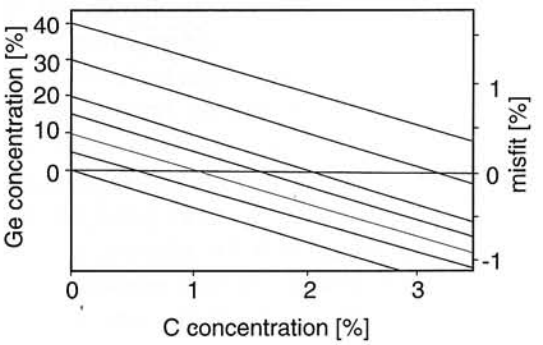

Fig. 2. Estimated misfit reduction in relation to Si for SiGe layers due to the presence of carbon in these layers (taken from Ref. 10).

3. Strained $Si_{1-x}Ge_x$/Si heterostructures

Si-based heteroepitaxy realized with the $Si_{1-x}Ge_x$ alloy means strained layer epitaxy. This results from the 4.17% lattice mismatch between Si and Ge. In the

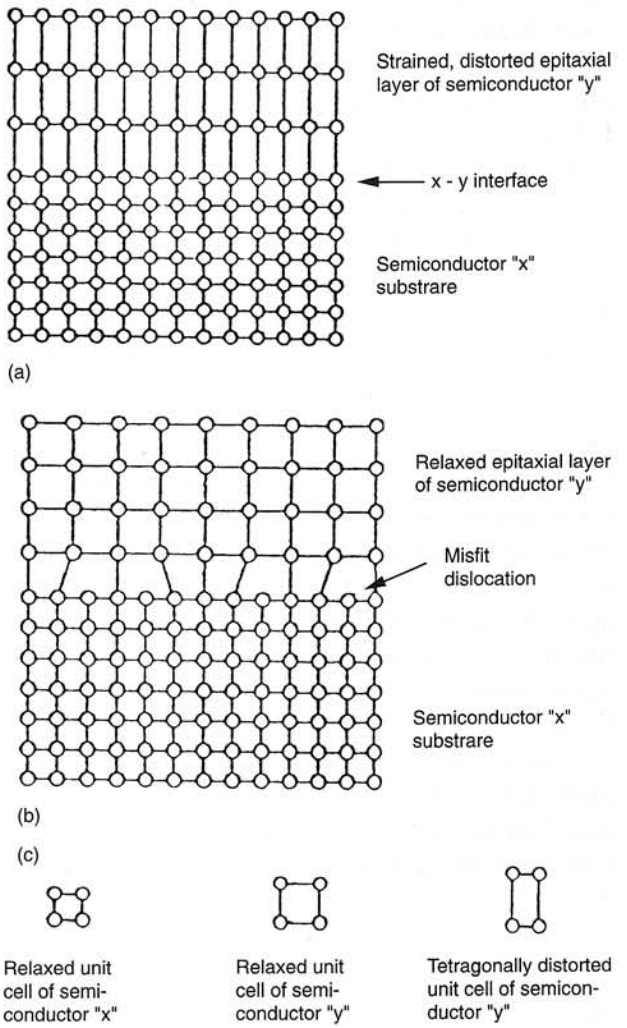

Fig. 3. Schematic illustrations of (a) strained and (b) relaxed epitaxial layer in the $Si_{1-x}Ge_x$/Si heterostructure, as well as (c) strained and relaxed unit cells (from Ref.11).

$Si_{1-x}Ge_x$ heterolayer a compressive strain occurs, which increases both for increasing Ge concentration in the alloy as well as for increasing the layer thickness. If the strain becomes too great, it will be relieved by the generation of dislocations in the interface area, which can severely degrade the device performance. A distinctive illustration of these effects is shown in Fig.3. In devices made of these heterostructures strain has the following electronic effects:

(i) energy band gap changes with strain; this can be used to tailor photodetector response,

(ii) energy band edge lineup in heterostructures depends on strain; this is the basis for various forms of charge carriers confinement in quantum wells of device structures (see Fig.4),

(iii) strain modifies the crystal symmetry; this offers the possibility of enhancing the radiative recom-

bination of electrons and holes in lasers and light emitting diodes, and

(iv) strain changes the coupling between various energy bands; this results in changes in carrier effective masses.

Multi-layer strained structures of Si and $Si_{1-x}Ge_x$ alloys are used to create electron/hole quantum wells, and thus allow modulation doping, which is not possible in conventional Si technology, and until recently was limited to III-V compounds [1]. The band alignment at the heterointerface of Si and SiGe is of type I, what means that the offset lies predominantly within the valence band (Fig.4a). To give an idea of the scale of this effect, the offset may be estimated at about 200 meV for $Si_{0.7}Ge_{0.3}$ commensurate to an underlying Si substrate [1]. On the other hand, when strained Si is grown on relaxed $Si_{1-x}Ge_x$ a staggered band alignment of type II results at the heterointerface (Fig.4b). In this case, the conduction band of $Si_{1-x}Ge_x$ is higher than that of Si (by about 200 meV for x = 0.3 in relaxed alloy), and the valence band in $Si_{1-x}Ge_x$ is lower than that of Si (by about 150 meV for x = 0.3).

The effect of strain [composition of the $Si_{1-x}Ge_x$ alloy ($0 \leq x \leq 0.7$) grown on relaxed $Si_{0.7}Ge_{0.3}$ buffer layer] on the energy of conduction and valence band edges may be seen in Fig.5. As a consequence of the shown band structure p-type modulation doping [3] can be achieved in both cases by doping the Si (or, more generally the low Ge-content layer) with acceptors, thus injecting holes in the highest Ge-content layer. N-type modulation doping, on the other hand, can only be achieved in the case of doping the relaxed high Ge-content layer with donors, segregating the electrons into the strained Si (more generally the low Ge-content) quantum well. In addition to the band offsets, the electron/hole effective masses are greatly affected by strain. Due to the strong anisotropy of the effective masses, energy bands with heavy masses are split from those with light masses. For lateral transport, it is desirable to have a light in-plane electron/hole effective mass in order to enhance the carrier mobility.

It is important to note that due to the quantization of the energy subbands of electrons/holes in the quantum wells, there is additional splitting of the effective masses. Bands with a heavy mass along the crystal axis (light in-plane mass) have a lower quantization energy, and, hence, the splitting due to the strain and that due to

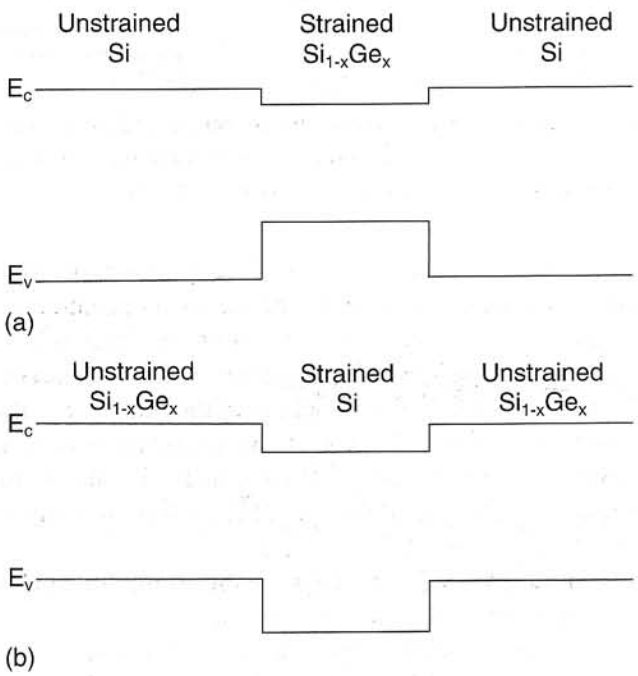

Fig. 4. Band edge lineup in Type I heterostructure (a) of a strained $Si_{1-x}Ge_x$ epilayer sandwiched between unstrained Si layers, and (b) in a Type II heterostructure of a strained Si epilayer sandwiched between unstrained $Si_{1-x}Ge_x$ layers (from Ref. 11).

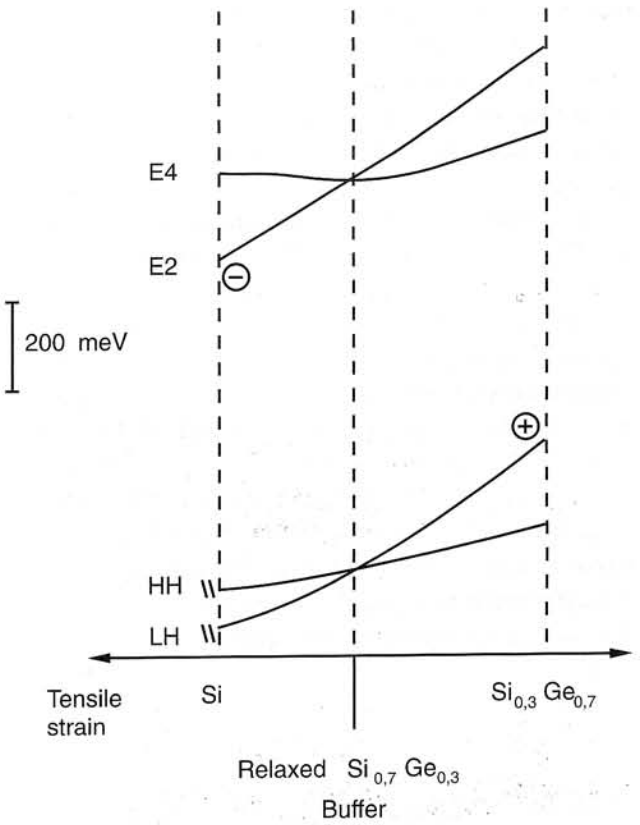

Fig. 5. Effect of strain on the conduction and valence band edges in $Si_{1-x}Ge_x/Si$. The substrate is assumed to be relaxed and to have 30% Ge in the alloy. The negative X-axis represents tensile strain and the positive one represents compressive strain with respect to the $Si_{0.7}Ge_{0.3}$ substrate (from Ref. 1).

quantization add. In the case of growing strained Si on relaxed $Si_{0.7}Ge_{0.3}$ the splitting of the two-fold degenerate energy band (E2) with light in-plane effective mass ($m^* = 0.2$ m) and the four-fold degenerate energy band (E4) with heavy in-plane electron effective mass ($m^* = 0.96$ m) is about 180 meV, large enough to have a profound effect on room temperature transport properties (only about 20 meV of this splitting is due to quantization in a 3 nm thick quantum well and the rest is due to strain). When a 3 nm thick $Si_{0.3}Ge_{0.7}$ quantum well is clad between relaxed layers of $Si_{0.7}Ge_{0.3}$, holes with light in-plane effective mass have an energy lower than holes with heavy in-plane effective mass. The above description of the valence band is, however, oversimplified, since the light hole mass applies only to the band edge and increases for higher energies due to the band nonparabolicity. Also at higher energy, the light and heavy hole bands mix resulting in a warped valence band. Nonetheless, high hole mobilities are achieved at room temperature employing such structures [1].

Heterostructures much more complicated than a single quantum well can be created by periodic variation along the growth direction of the $Si_{1-x}Ge_x/Si_{1-y}Ge_y$ ($0 \le x,y \le 1$) alloy composition with the period shorter than the electron mean free path in the solid. In such structure, called strained-layer superlattice (SLS), the epilayers are strained. Thus, (SLS) are structures comprising alternating layers of two o more materials with different equilibrium lattice constants, grown in a structure with a common in-plane (lateral) lattice constant (Fig. 6). The mismatched layers of the SLS are purely accommodated by strain, what means that the thicknesses t_1 and t_2 of the individual superlattice layers meet the requirements of pseudomorphic growth [3] (t_1, $t_2 < t_c$, the critical thickness for generation of misfit dislocations). While the SLS as a whole exhibits the same lateral lattice constant a_{lt} (parallel to the interfaces) equal to

$$a_{lt} = a_1(1 + \varepsilon_1) = a_2(1 + \varepsilon_2) \qquad (4)$$

the strain changes abruptly by the amount $(\varepsilon_2 - \varepsilon_1)$ at each interface between adjacent layers. However, the strain distribution is determined by the choice of the lattice constant a_{lt}.

It has been shown [7] that a SLS is stable as a whole against the introduction of misfit dislocations if the strain is symmetrized according to the relation

$$\varepsilon_1 = -\varepsilon_2 = (a_2 - a_1) / (a_1 + a_2) \qquad (5)$$

Here, the term strain symmetrization is used for SLSs with equal layer thickness $t_1 = t_2 = L/2$, where L is the spatial period of the SLS. In the case of strain symmetrization, there is no limiting critical thickness t_{cs} of the superlattice as a whole ($t_{cs} \to \infty$). However, if the strain is asymmetrically distributed the SLS can gain energy by introduction of misfit dislocations at its base if the thickness of the superlattice (NxL), where N gives the number of periods of the SLS, exceeds the critical superlattice thickness t_{cs}. The t_{cs} will decrease with increasing asymmetry of the strain distribution. The extreme case with the lowest t_{cs} is achieved if only one material in the SLS is strained (this occurs when a $Si_{1-x}Ge_x/Si$ SLS is directly grown on a Si substrate without a strain-adjusting buffer layer [7]). In the case of a thin (≤ 0.25 μm), homogeneous buffer layer, whose strain-adjusting misfit-dislocation network is mainly confined to the interface between substrate and buffer layer the in-plane lattice spacing a_{lt} is controlled by the lattice constant a_B of the buffer material and by the strain ε_1 in the buffer. The latter depends on the mismatch between substrate and buffer layer, as well as on the buffer-layer thickness.

$$a_{lt} = a_B (1 - \varepsilon_B) \qquad (6)$$

The design of the buffer layer is explained here exemplarily for a $Si_{1-y}Ge_y$ buffer layer on a Si substrate.

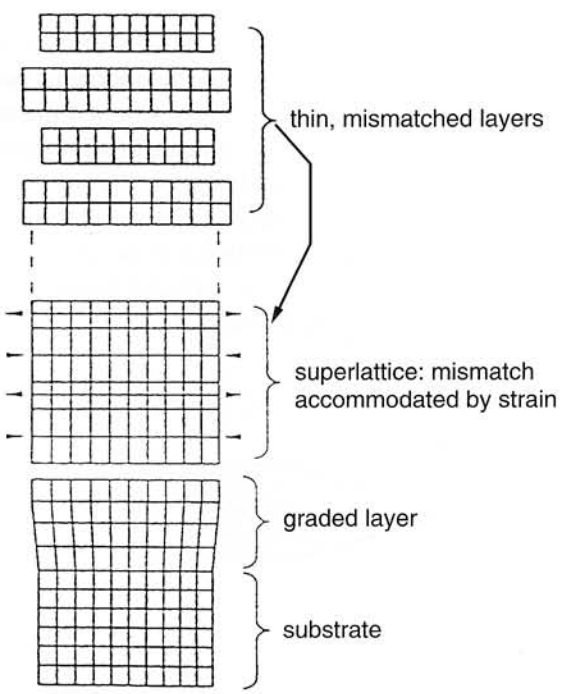

Fig. 6. Schematic illustration of the elements and formation of an SLS (taken from Ref.12).

With the lattice mismatch between Ge and Si being 4.2%, and assuming Vegard's law, we get for the lattice constant of the buffer layer as a function of the chemical composition y,

$$a_B = a_A\,(1 + 0.042y) \qquad (7)$$

where a_A stays for the substrate lattice constant.

4. Photodetectors made of $Si_{1-x}Ge_x$/Si heterostructures

Quality and design of photodetectors play a significant role in the systems in which they are used [4]. For example, in fiber-optic communication,the capacity of an existing system can be increased by changing one type of photodetector with another. For this application, the detector must have high gain and large bandwidth centered at a wavelength where the fiber exhibits minimum losses. For night vision devices, dynamic range must also be large.

4.1. p-i-n photodetectors

Most fiber-optic systems around the world have used p-i-n photodetectors, usually made of Si, however, more recently $Si_{1-x}Ge_x$ strained layer photodiodes have been fabricated and used, too [4]. Let us take as an example of such photodiodes the p-i-n detector with pseudomorphic 20 period $Si_{1-x}Ge_x$/Si superlattice MBE-grown on a Si(100) substrate. The schematic diagram of the structure of this photodetector is shown in Fig.7. The thickness of the $Si_{0.4}Ge_{0.6}$ quantum wells of the superlattice was equal to 60 Å,while the thickness of the Si barrier layers was equal to 250 Å. The superlattice was sandwiched between n- and p-type Si layers. A thin p^+ Si contact layer was deposited on the top of the detector for making the ohmic contact. The detector was illuminated from the edge by unpolarized light from a 5 to 8 μm diameter optical fiber. The coupling efficiency between the fiber and the superlattice was about 20% while the light within the superlattice structure was guided by total internal reflection, what caused an increase in the absorption path. The breakdown voltage of the diode was between 30 and 38V and the internal peak efficiency was at the wavelengths near 1.3 μm. equal to 47%,while the overall external efficiency was 10%. Studies optimizing the superlattice dimensions and periodicity show that the configuration of the detector was nearly optimal [4].

4.2. Detectors based on intersubband absorption in quantum wells

If the thickness of a quantum well is small, the energy bands of the semiconductor creating the well layer split into subbands. Due to the quantum size effect the separation between the subbands on the energy scale can be changed by changing the well width. The optical absorption between the subbands of either the conduction or the valence band gives rise to photoconduction, thus, the quantum well absorption can be used for photodetection. The quantum well infrared photodetectors (QWIPs) are tunable and exhibit high quantum efficiency,they have high detectivity, and high responsivity [4].

The key features of a p-$Si_{1-x}Ge_x$/Si QWIP detector are illustrated in Fig.8. The alloy layers are grown pseudomorphically [3] on a Si substrate, and are compressively strained. The alloy bandgap is smaller than that of Si, the difference at low temperature being $\Delta E_g = 896x - 396\,x^2$ meV for fully strained material [14]. This bandgap difference appears almost entirely as an offset at the valence band edge, so that $\Delta E_v \sim \Delta E_g$. The strain lifts the degeneracy of the light and heavy holes at the center of the Brillouin zone in the alloy well layer, the lowest energy subband being heavy-hole like with confinement energy E_1 in the well. The

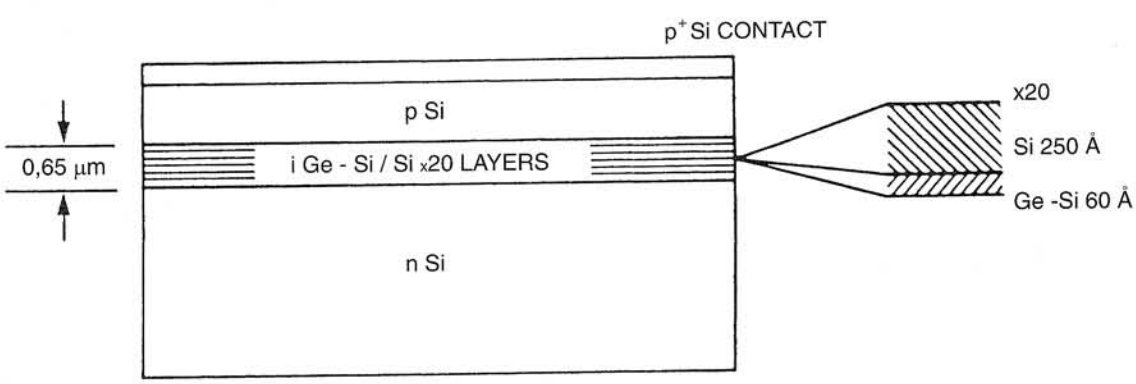

Fig. 7. Schematic diagram of the structure of a p-i-n photodetector $Si_{0.4}Ge_{0.6}$/Si SLS (taken from Ref.13).

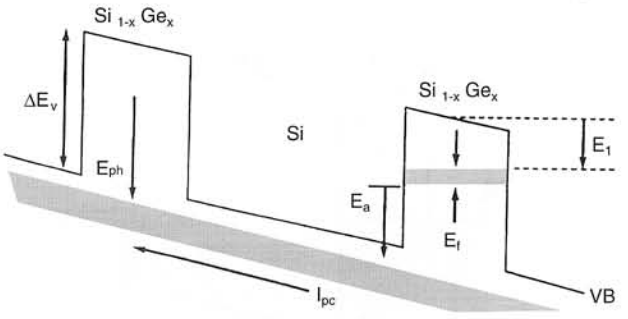

Fig. 8. Schematic valence band diagram for a p-$Si_{1-x}Ge_x$/Si QWIP under bias. The symbols are explained in the text (taken from Ref.14).

alloy exhibits a 2D density-of-states so that p-type doping of the well gives a Fermi energy $E_f = n_s\pi\hbar^2/m^*$, where n_s is the sheet doping concentration, m* is the hole effective mass, and $\hbar$ is the Planck's constant divided by 2π.

The Si barrier layers are made thick (typically 30 – 50 nm) in order to minimize tunnelling of holes between quantum wells; carriers trapped in the well layer then cannot move in response to a bias applied in the growth direction perpendicular to the layers. However, states above the barrier edge have a three-dimensional density-of-states and carriers which are thermally excited can be collected under the applied bias, generating a thermal dark current with activation energy E_a. Carriers are also photoexcited to the barrier states by infrared photons of energy E_{ph} and generate a photocurrent, I_{ph}. The spectral response can be tuned by varying the Ge fraction x in the alloy, which determines ΔE_v, and by changing the well width which determines E_1. For a typical 8 nm wide well layer used in this QWIP the confinement energy E_1 was < 10 meV, which is small compared with photon energies > 100 meV. A schematic cross-section of a mesa – isolated QWIP made in the form of a 50-period quantum well structure,with Si barrier layers nominally 50 nm thick and the well layers of p-$Si_{1-x}Ge_x$ nominally 4 nm thick, exhibiting sheet doping concentrations in the range $0.1 - 0.8 \times 10^{12}$ boron atoms per cm^{-2} is shown in Fig.9. The mesa of the diode was typically 1 mm in diameter, with the aluminium top contact covering less than half the mesa's area to allow normal incidence optical excitation.

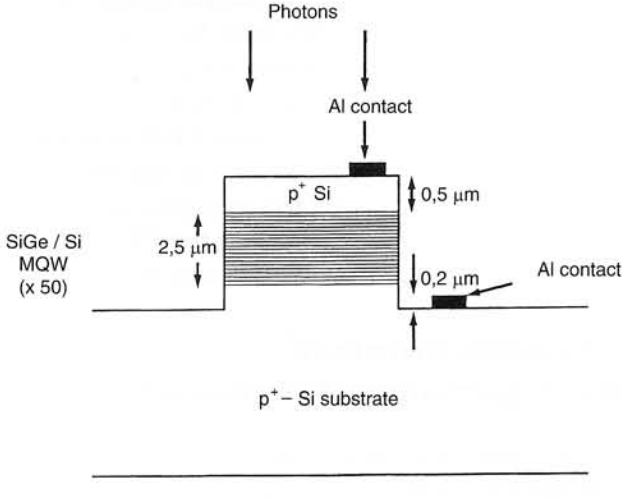

Fig. 9. Schematic cross-section of a mesa-isolated QWIP. The infrared radiation is normally – incident on the top surface. The p^+-Si substrate absorbs radiation passing through the active multiple quantum well region (taken from Ref.14).

QWIP diodes of the type described above have been grown and characterized, as described in Ref.14. Good control of periodicity in these pseudomorphic multiple quantum well structures on Si substrates was demonstrated by real-time ellipsometry during growth processes and subsequently confirmed by transmission electron microscopy. The photoresponse spectrum was tuned in the 8 – 13 μm waveband by varying the Ge fraction in the $Si_{1-x}Ge_x$/Si quantum wells. Dark currents were reduced by doping only the center regions of the quantum wells. The devices reported in [14] worked with only a single pass of the incident radiation, thus, further work will be necessary to increase the optical coupling efficiency in order to increase the operating temperature significantly above 50 K. Then the favorable material properties of the $Si_{1-x}Ge_x$/Si heterostructures will make them good candidates for high resolution , high performance infrared focal plane arrays.

4.3. Heterojunction internal photoemission detectors

Heterojunction internal photoemission (HIP) effect consists in photoexcitation of carriers (holes or electrons) across the energy barrier occurring at the hetero-interface, what causes the emission of these excited carriers from the illuminated material of the hetero-pair to the other one. Energy band diagram and structure of a p^+- $Si_{1-x}Ge_x$/p-Si HIP photodetector is shown in Fig.10. A 10 nm thick boron doped (5×10^{20} cm^{-3}) $Si_{0.7}Ge_{0.3}$ layer was grown epitaxially on top of a p-type Si substrate. The heterojunction barrier suppresses the dark current and determines the cutoff wavelength of the device, which can be varied by changing the Ge content in the alloy. The optical barrier was determined to be 54 meV for this device, corresponding to a cutoff wavelength of 23 μm. [15]. The advantage of the HIP photodetectors over the ma-

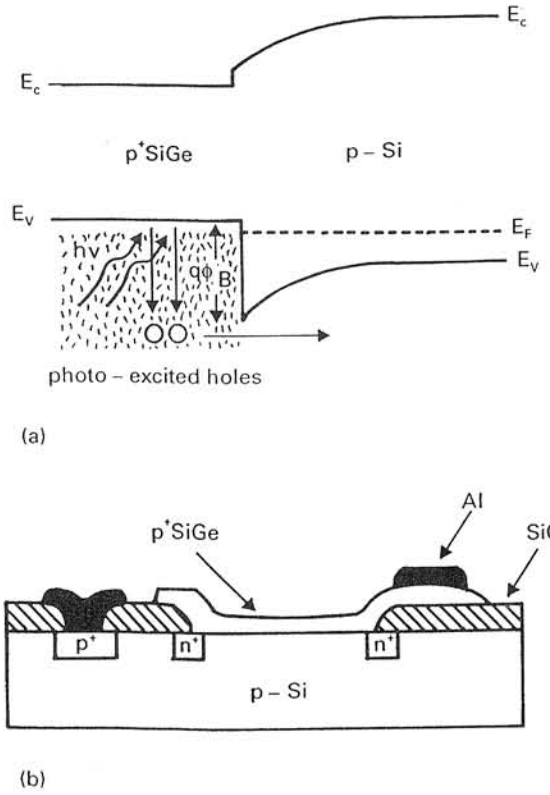

Fig. 10. Energy band diagram (a) and the structure (b) of a p^+-$Si_{1-x}Ge_x$/p-Si HIP photodetector. The n^+ regions act as guard rings and define the active area of the device (taken from Ref.5).

ture silicide/Si Schottky barrier photodetectors is that the cutoff wavelength can be in principle tailored over the range 3-30 μm for the SiGe/Si material system. The described photodetector has outperformed an IrSi photodetector with the same cutoff wavelength with regard to quantum efficiency and dark current.

A promising variant of HIP photodetectors is the so called tunable infrared photoemission sensor (TIPS) [16]. It consists of two different conducting materials (metal or p-type degenerately doped $Si_{1-x}Ge_x$) separated by a thin undoped Si layer. The two conducting materials are chosen with different barrier heights on silicon (either Schottky barrier heights or heterointerface barrier heights due to valence band discontinuities) such that the depleted Si layer forms an asymmetrical potential barrier to the carriers (both, holes and electrons) photocreated in each conducting film. Under sub-band illumination, the photo current flowing between the two conducting films is therefore strongly dependent on the shape and height of the Si potential barrier, that can be varied by a small bias (less than 1V) applied between the two electrodes.

The first TIPS device has been demonstrated

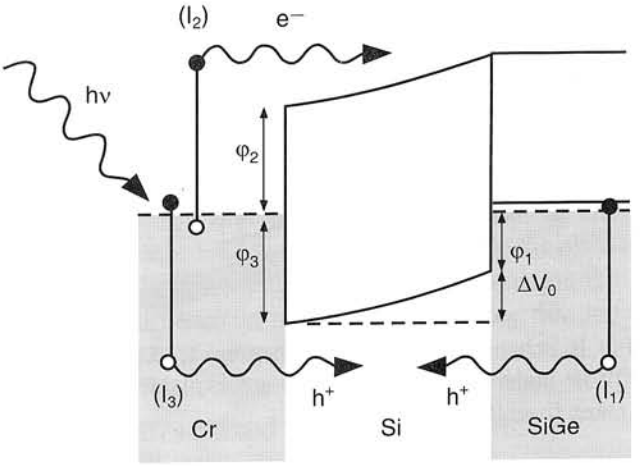

Fig. 11. Energy band diagram of the Cr/Si/ p^+-$Si_{1-x}Ge_x$ TIPS with no applied bias (taken from Ref.16).

using the Cr/Si/p^+-$Si_{0.86}Ge_{0.14}$ heterostructure in which the Si/p^+-SiGe layers are grown epitaxially on a silicon substrate, and the top metal layer (Cr) is deposited by high vacuum evaporation [16]. The energy band diagram of this TIPS device, with no applied bias, is shown in Fig.11. The three photoemission processes are schematically represented by: I_1 (holes from SiGe towards Cr) and I_2 (electrons from Cr towards SiGe) which are specific to the TIPS structure, and I_3 (holes emitted from Cr below the Si barrier towards SiGe) which is similar to the photoemission process observed in a Schottky diode. The experimental data concerning external quantum efficiency (number of carriers collected on the electrodes by incident photon) of the described TIPS are shown in Fig. 12. The observed photoresponse tunability of the SiGe TIPS may be quantitatively explained by the effective barrier height (EBH) variation more than 10 times larger than the standard Schottky barrier lowering because EBH is equal in the first approximation to the sum of the SiGe/p-Si barrier height and the potential drop present in the Si layer. The wavelength tunability of the TIPS has also been confirmed by I-V measurements [16].

5. Epitaxial growth of silicon-germanium heterostructures

Two epitaxial growth techniques figure prominently in the field of $Si_{1-x}Ge_x$/Si heterostructures epitaxy. These are solid source molecular beam epitaxy (SS MBE) and ultrahigh vacuum chemical vapor deposition (UHV CVD) [5]. Let us discuss both of them in short.

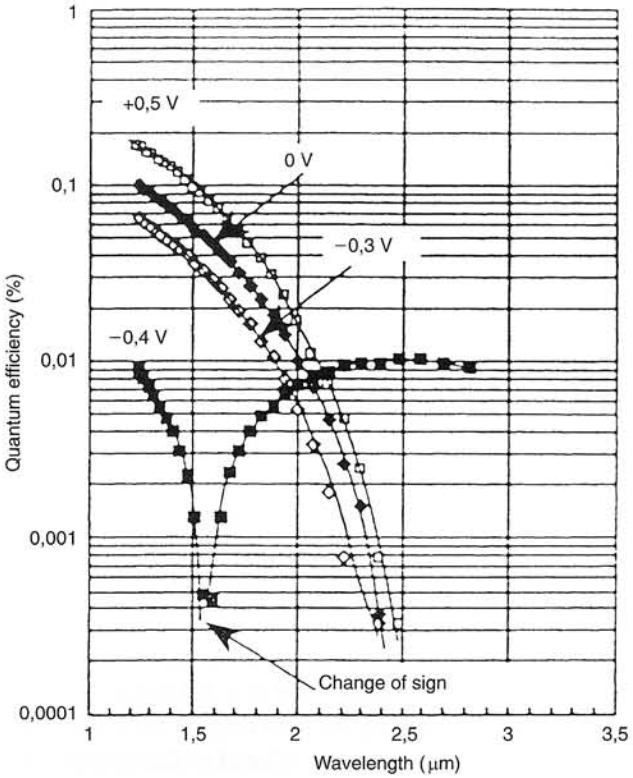

Fig. 12. External quantum efficiency as a function of wavelength of the SiGe TIPS structure decribed in the text, measured at 77K on a square diode of 0.17 mm^2 active area at low positive and negative biases. The structure is back illuminated, i.e., on the Si substrate. (from Ref.16).

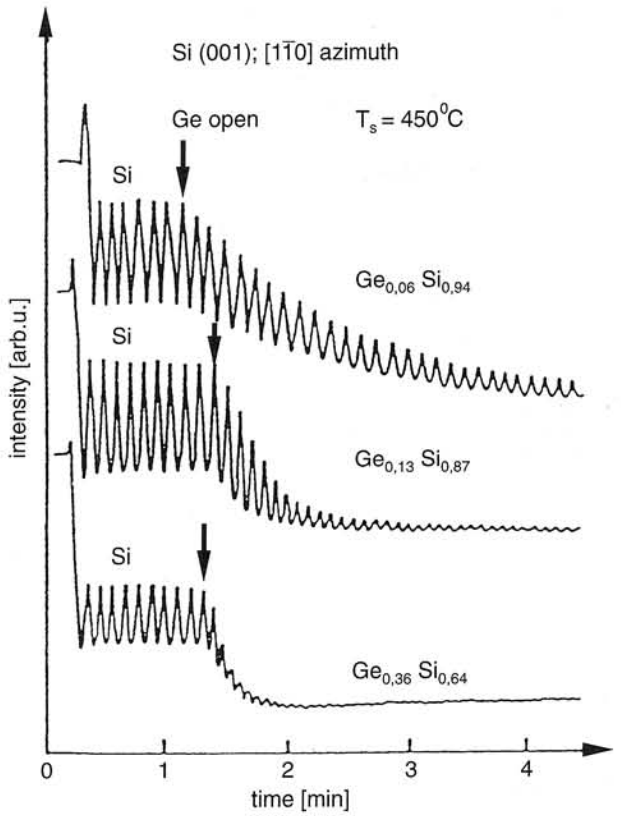

Fig. 13. RHEED intensity oscillations of the specular beam during growth of $Si_{1-x}Ge_x$ on Si(001) at 450°C taken from the [110] azimuth for various Ge mole fraction. The Si growth (stable oscillation amplitude) preceded the alloy growth (from Ref.3).

5.1. MBE growth

At present, SS MBE is capable of growing Si epitaxial layers on large area substrates (exceeding 200 mm in diameter) with deposition uniformity better than ± 1.5%, high crystal quality, and arbitrary, well-controlled doping profiles. Also the quality of $Si_{1-x}Ge_x/Si$ heterostructures has been considerably improved by using a Reflection High Energy Electron Diffraction (RHEED) oscillation monitoring and controlling technique during MBE growth [17].

One of the fundamental problems in Si MBE is the appropriate substrate preparation. In contrast to the conventional crystal growth techniques, MBE cannot employ melt-back or chemical etch-back to generate a clean, well-ordered substrate surface. Works on substrate preparation techniques have concentrated on two areas: a reexamination of the established procedures of ex situ chemical cleaning and in situ sputter etching; and developments of new procedures such as UV ozone processing and in situ reduction of surface oxides by silicon deposition [3]. It has been known for some time that a perfectly clean silicon surface has a strong affinity for carbon, and that once formed these bonds are extremely hard to break. Chemical cleaning procedures are, therefore, aimed at generating a passivating surface oxide layer rather than a clean silicon surface. The most important conclusions concerning Si substrate preparation for MBE may be formulated as follows:

– the substrate must be annealed prior to MBE growth at a temperature much higher than the growth temperature in order to obtain stable RHEED intensity oscillations (see Fig.13).

- with an increase of annealing temperature and time, the amplitude of the oscillations increases and their period doubles. That means a change of the reconstruction of the annealed surface from a two-domain structure (2×1 and 1×2) to a (2×1) single domain structure.

The $Si_{1-x}Ge_x/Si$ heterostructures and superlattices may be grown in typical Si MBE systems. Two examples of such systems are schematically shown in Figs. 14 and 15. The details of MBE growth of these

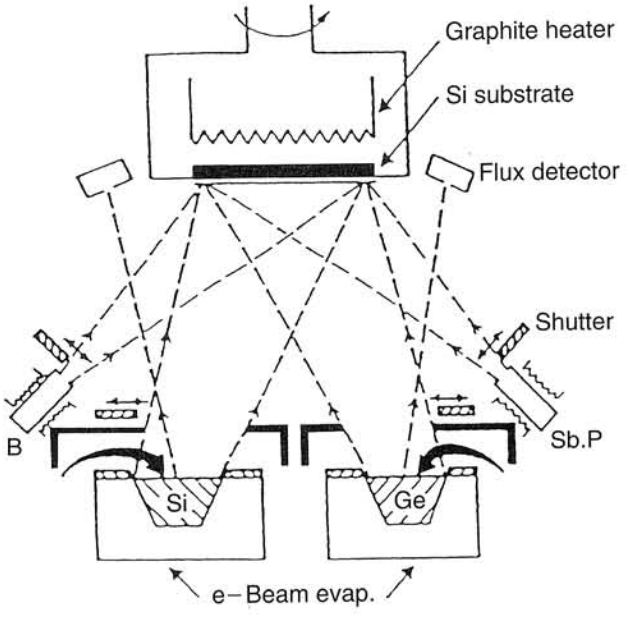

Fig. 14. The major components of a solid-source MBE system. Shown are the collimated electron-beam sources for Si and Ge fluxes, the Knudsen cells for B, Sb and P dopants, shutters for interrupting matrix and dopant deposition, heated substrate and substrate rotation (from Ref.5).

structures are given in [3] and [17]. Films of $Si_{1-x}Ge_x$ with various Ge mole fractions may be grown by controlling the evaporation rate of a Si source and that of a Ge source. Typical RHEED intensity oscillations of a specular beam observed from the [110] azimuth at 450°C are shown in Fig.13. The growth of $Si_{1-x}Ge_x$ was preceded by Si growth for several oscillations in order to determine the alloy composition. While the oscillation amplitude and the average intensity were almost unchanged during Si growth, they began to decrease after $Si_{1-x}Ge_x$ growth started. The decrease was more rapid with an increase in the Ge mole fraction in the grown film. In the growth of Ge on Si at 450°C, i.e., x = 1.0, only two periods of oscillation were observed. The damping behavior of the oscillations could be explained by clustering during $Si_{1-x}Ge_x$ growth as follows: when the Ge mole fraction was small, the RHEED pattern during $Si_{1-x}Ge_x$ growth was almost the same as that during Si growth. However, with an increase in the Ge mole fraction, the RHEED pattern rapidly changed from the initial streaky type to the final spotty type. It was concluded from these observations of RHEED patterns that the decrease of the oscillation amplitude during $Si_{1-x}Ge_x$ growth was a result of a change in the growth mode from a two-dimensional layer-by-layer type to a three-dimensional type which is caused by a clustering of $Si_{1-x}Ge_x$. The motive force for clustering is related to the lattice mismatch between Si substrates and $Si_{1-x}Ge_x$ epilayers.

To characterize the MBE growth of strained layers two kinds of critical thickness are generally mentioned [3]. t_c is the thicknesses above which misfit dislocations are generated and t_{3D} is the onset of three-dimensional (3D) growth. It has been shown that nonequilibrium conditions achieved with MBE generally lead

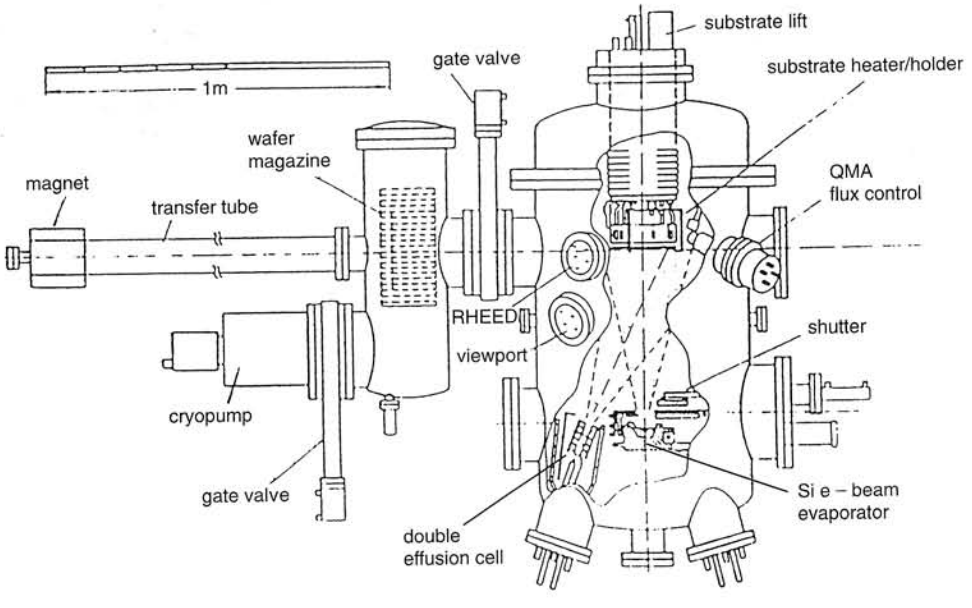

Fig. 15. Cross-sectional view of a modern Si-MBE machine consisting of a growth chamber (right) and a storage chamber for a cassette-type substrate magazine. For reasons of clarity, the pumping system of the growth chamber is not shown (from Ref.7).

to experimental critical thicknesses which are very dependent on the growth conditions; especially the growth temperature. Consequently, metastable pseudomorphic layers much thicker than the equilibrium critical thickness can be obtained, and there is a need to define experimentally the actual thickness at which strain begins to be relieved. The RHEED technique has been widely used to directly measure, in situ, t_{MD} and t_{3D} during MBE growth. The most important conclusions resulting from RHEED investigations on strained-layer MBE may be summarized as follows: (i) two completely different relaxation mechanisms, misfit dislocations or 3D island dislocations, are expected to exist depending on whether the growth mode is 2D or 3D. These mechanisms are strongly temperature dependent. Low growth temperature reduces the kinetics of dislocation motion which consequently minimizes interaction and multiplication of dislocations and deletes the plastic relaxation. On the other hand, the transition from 2D growth to 3D islands is directly related to variations of the temperature dependent mobility of surface atoms. Decreasing the growth temperature deletes 3D growth and therefore the plastic relaxation, (ii) weak RHEED oscillations are associated with a quasi layer-by-layer growth mode with large 2D islands. Eventually, these 2D islands transform into 3D coherent islands before relaxing. This behavior is explained using thermodynamic and energy conservation considerations. It is recognized that at thermodynamic equilibrium the surface of minimum free energy of strained epilayers is not atomically flat, but is three dimensional in form, (iii) growing at higher temperature favors near-equilibrium conditions and the appearance of a 3D growth mode for highly strained layers. In contrast, lowering the temperature forces a 2D growth mode, due to a decrease of the interplane mobility of surface atoms. The 2D/3D growth mode transition occurs when the energy lost by increasing the surface energy, when going from 2D to 3D, becomes smaller than the energy which will be gained by decreasing the bulk strain energy through elastic relaxation of 3D islands [18].

In order to increase the thickness of the pseudomorphically grown epilayers much over the equilibrium t_c different MBE growth techniques have been invented [3]. Among them the earliest applied was the Phase-Locked Epitaxy technique of Sakamoto et al. [19]. The idea of this technique is as follows. The intensity oscillations of the specular beam in the RHEED pattern is recorded during the MBE growth process from the fluorescent screen of the difractometer system in the MBE machine by a photo-detecting system. The phase of these oscillations is continuously analyzed by a computer which controls also the operation of effusion cell shutters. According to the physical principle of the so-called "recovery effect" [9] (during the growth interruption time, the specular beam intensity in the RHEED pattern increases, what is attributed to surface smoothing of the grown epilayer caused by increased adparticles migration or sublimation) the growth is interrupted by the computer when only the amplitude of the RHEED oscillations starts to decrease, and is initiated again when it recovers to the initial value during the growth interruption time. By repeating the brief growth interruptions periodically, in synchronism with the monolayer-by-monolayer growth sequence, the amplitude of the resulting oscillations will persist and not damp out with time. The optimum timing for the periodic growth interruptions improves the flatness of the epilayer growth front, which is smoothest just after a RHEED specular beam reached its maximum. In the year 1991, the idea of MBE with phase synchronization, as applied to elemental group-IV semiconductors Si and Ge, was demonstrated by Markov et al. [20]. The application of this technique to MBE growth of $Si_{1-x}Ge_x$ / Si(111) heterostructures resulting in considerable improvement of their heteroepitaxial growth was demonstrated by Larsson and Hansson [21].

With the help of the oscillation recovery effect, Sakamoto et al. [3] were able to apply a "phase-locking technique" to the growth of a $Si_{1-x}Ge_x$/Si strained-layer superlattice on a Si(001) substrate. They obtained 26 periods of a $(Si_{0.75}Ge_{0.25})_{10}/Si_{10}$ strained-layer superlattice, i.e., 520 atomic layers (70 nm), while monitoring the RHEED intensity oscillations. The total thickness of the $Si_{0.75}Ge_{0.25}$ layers (35 nm) was much larger than the critical thickness for the relevant Ge mole fraction (~8 nm). The $Si_{1-x}Ge_x$/Si interfaces in the strained-layer superlattice grown on the Si(001) substrate using this technique were examined by High-Resolution Transmission Electron Microscopy (HRTEM).

The RHEED intensity oscillation and the HRTEM image showed a difference in roughness between a $Si_{1-x}Ge_x$ on Si interface and a Si on $Si_{1-x}Ge_x$ interface. This suggests that it is necessary to use a $Si_{1-x}Ge_x$ on Si interface in order to improve the electrical properties of, e.g., a modulation-doped structure. Similar results were obtained on the strained-layer heterostructure of $Si_{1-x}Ge_x$/Si(111).

Another interesting feature of $Si_{1-x}Ge_x$/Si heterostructures MBE, is the smoothening of the alloy surface during Si overgrowth. The Ge growth was stopped and the Si source shutter was opened after the

RHEED pattern changed to a spotty type indicating a rough Ge surface. Although no oscillations could be observed at the beginning of the Si overgrowth, a weak oscillation appeared and gradually gained in amplitude with an increase in the Si-overgrown layer thickness. One may consider from this result that the atomically rough surface from the three-dimensional growth of Ge was smoothed during the initial stage of Si overgrowth by Si atoms; then, the RHEED intensity oscillation was observed on the smoothed Si-overgrown surface.

Creating heterostructures is often an exercise in defeating the growth mode of an epitaxial layer [18]. At sufficiently high temperatures to ensure epitaxy, the surface layer is, by necessity, quite mobile. This mobility allows the film to attain a thermodynamically stable structure, dictated by the combination of surface and interface free energies and the lattice strain of the heterolayer. If one attempts to grow an overlayer that has a higher surface free energy than the underlying medium, the overlayer will island rather than wet the surface. In growing an embedded layer, first a heterolayer must be formed, followed by a capping layer of the substrate species. Only one of these two species can have the lowest surface free energy of the two. Thus, in growing an embedded layer, either the growth mode of the heterolayer, or the capping layer will be Volmer-Weber (i.e., immediate islanding). Thus, if material A wets material B, B will not wet A. Any attempt at growing an A/B/A heterostructure must overcome this fundamental obstacle [3]. Furthermore, should there be significant lattice mismatch, island formation, strain-enhanced diffusion, and/or defects may arise after some critical thickness has been grown. Copel et al. [22] proposed the use of a surface-active species, so called surfactant, to reduce the surface free energies of A and B and suppress island formation, as demonstrated in the growth of Si/Ge/Si(001) with a monolayer of As. The idea was to gain control over growth by manipulation of surface energetics what should provide a new avenue to achieve high-quality man-made microstructures against thermodynamics odds [18].

An interesting effect, the increase of the $Si_{1-x}Ge_x/Si$ interface abruptness in a quantum well (QW) has been found, when growing the QW by surfactant-mediated MBE (SM MBE) with Sb as the surfactant [23]. Sputter depth profiles of Ge atoms of the QW structure, measured by a secondary ion mass spectrometer (SIMS) have clearly evidenced that Ge atoms segregate to the surface in the sample without Sb adlayer. This segregation is inherent to a $Si/Si_{1-x}Ge_x$ heterointerface grown by MBE in favor of surface energetics. In contrast SM MBE sample exhibits no segregation edge. This remarkable change in the depth profile of Ge atoms evidences that the Sb adlayer effectively suppresses the surface segregation of Ge. Thus, an abrupt $Si/Si_{1-x}Ge_x$ interface can be created in MBE growth, with interface transience better than 0.4 nm in terms of the decay length of the Ge content.

5.2. UHV CVD growth

The technique of chemical vapour deposition (CVD) relies on the decomposition of gaseous precursors on a heated substrate, most usually involving reduction of chlorosilanes (e.g. $SiCl_4$) or pyrolytic decomposition of silane (SiH_4). There are several variants of this method characterized by the pressure of gases used, the temperature and the method of heating the substrate and the temperature of the walls of the chamber with respect to the substrate. In the "cold wall" situation this temperature is low compared to the substrate and in the "hot wall" situation they are the same. In all cases the rate of decomposition and doping are determined by the substrate temperature (T_s), generally increasing with T_s and there is a complex interdependence of matrix and doping levels. Over recent years there have been considerable advances in the understanding of surface chemical processes central to CVD, which have enabled predictable and high quality growth to take place at low temperatures and pressures that were hitherto not possible. High material quality is generally readily achieved in CVD by adopting UHV practices to reduce gaseous impurity uptake at the lower growth temperatures. Also, there have been considerable technological improvements in CVD systems over the last few years, enabling rapid control of gas compositions and of the substrate temperature. Indeed a version known as rapid thermal processing (RTP). CVD allows the wafer temperature to be rapidly ramped up and down to enable very thin layers (down to 5 nm) to be grown [5]. Multichamber CVD systems are available, enabling hitherto incompatible growth schedules (e.g. high/low doping sequences) to be achieved by this growth technique. Another version of CVD and one favoured by some companies piloting HJBT production is UHV-CVD (Fig.15) developed by Meyerson at IBM, and comprising a system constructed to UHV standards, and operating at low pressures [5]. Many wafers can be loaded simultaneously and with the growth furnace (growth chamber plus wafers) at the growth temperature (between 550-850°C) matrix and dopant gas mix-

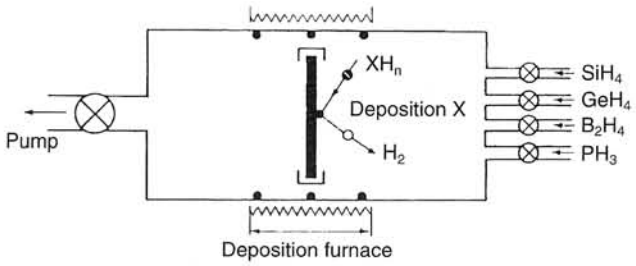

Fig. 16. Schematic illustration of a UHV-CVD system for SiGe growth and doping (taken from Ref.5).

tures are admitted for the growth period. With appropriate control and rapid pumping of the gas mixtures (e.g. SiH_4, GeH_4, B_2H_6, PH_3) high quality layers down to 1.5 nm in thickness have been demonstrated. As with all single chamber CVD techniques it does suffer from memory doping effects making it difficult to maintain well controlled doping at low concentrations after high levels of doping have taken place. An important advantage of CVD techniques is that deposition can be restricted to selected areas of the wafer (selective-epitaxy). The potential for batch processing has attractions for industry and IBM are using UHV-CVD for HJBT pilot production. UHV-CVD is obviously suited to a production environment, and commercial systems are just starting to become available (Leybold AG).

5.3. Estimation of the MBE and UHV CVD growth techniques

The relative merits of the various epitaxy processes are difficult to assess. With appropriate safeguards high material quality can be achieved by all variants of CVD and MBE. The C and O levels are critically dependent on growth temperature in both CVD and MBE and adoption of UHV standards of system cleanliness pays dividends in this respect. CVD epitaxy is a process acceptable to the silicon industry whereas MBE epitaxy has yet to make inroads. In well designed systems which may well involve single wafer processing in the future, the key attribute of both CVD and GS-MBE is likely to remain selective growth capability and that of SS-MBE flexibility in matrix and dopant profile control.

SiGe epitaxy still remains a formidable challenge to growers. There is considerable difficulty in producing high quality structures on Si substrates with Ge concentrations $\geq 30\%$ by either MBE or CVD. Ge tends to segregate, producing smeared interfaces, and surface rippling tends to occur which is associated with the minimization of the strain energy in the layer.

6. Conclusions

It is a remarkable fact that after only about twenty years of investigation in a laboratory scale of the epitaxial growth of $Si_{1-x}Ge_x/Si$ strained layer heterostructures, this material system is now engaging the attention of circuit and process engineers with the heterojunction bipolar transistor set to enter the marketplace [5], [24]. On the optical side the infrared detectors using $Si_{1-x}Ge_x/Si$ heterostructures seem to have a commercial impact soon. This concerns mainly far infrared detectors, i.e., QWIP and HIP detectors, operating in the atmospheric window wavelength range of 8-14 μm. [5], [14]. However, new designs and constructions are still proposed [16], [25], [26], concerning the medium infrared atmospheric window (3-5 μm) and the near infrared optical fiber communication window (1.3-1.6 μm.).

Looking further ahead, silicon will almost certainly continue to dominate semiconductor microelectronics for the next twenty years and more, penetrating also into semiconductor optoelectronics. As dimensions reach 0.1 μm and below radically new concepts will be needed to perform active device functions. "Quantum wires" and "quantum dots" in which carriers are confined to one and zero dimensions are currently under investigation in many laboratories. Ultra-small capacitance devices involving single electron action are also under consideration. Where these and more conventional devices involve silicon, it would be very surprising if silicon-germanium/silicon heterostructures did not have an important role to play.

References

1. K.Ismail and B.S.Meyerson: *Si/SiGe quantum wells: fundamentals to technology.* J. Mater. Sci.: Materials in Electronics **6** (1995) 306.
2. E.Kasper, H.J.Herzog and H.Kibbel: *A one dimensional SiGe superlattice grown by UHV epitaxy.* Appl. Phys. **8** (1975) 199.
3. M.A.Herman and H.Sitter: *Molecular Beam Epitaxy – fundamentals and current status, 2nd.ed., (Springer, Berlin, Heidelberg, 1996).*
4. S.C.Jain: *Germanium-Silicon strained layers and heterostructures,* (Academic Press, Boston, San Diego, 1994).
5. T.E.Whall and E.H.C.Parker: *Silicon-germanium heterostructures – advanced materials and devices for silicon technology.* J. Mater. Sci.: Materials for Electronics **6** (1995) 249.

6. M.A.Herman: *Silicon-based heterostructures in optoelectronics.* Opto-Electr. Rev. **4** (1996) 77.
7. E.Kasper and F.Schäffler: *Group-IV Compounds,* in Semiconductors and Semimetals, R.K.Willardson and A.C.Beer (eds.), **33** (1991) chapt. 4.
8. S.C.Jain, H.J.Osten, B.Dietrich and H.Rücker: *Growth and properties of strained* $Si_{1-x-y}Ge_xC_y$ *layers.* Semicond. Sci. Technol. **10** (1995) 1289.
9. E.Kasper, A.Schuh, G.Bauer, B.Holländer and H.Kibbel: *Test of Vegard's law in thin epitaxial SiGe layers.* J. Cryst. Growth **157** (1995) 68.
10. H.J.Osten, B.Dietrich, H.Rücker and M.Methfessel: *Local structure of strain-compensated epitaxial* $Si_{1-x-y}Ge_xC_y$ *layers Si(001) grown with molecular beam epitax.* J. Cryst. Growth **150** (1995) 931.
11. K.I.Wang, S.G.Thomas and M.O.Tanner: *SiGe band engineering for MOS, CMOS and quantum effect device.* J. Mater. Sci.: Materials in Electronics **6** (1995) 311.
12. P.S.Peercy: *Strained-layer superlattices,* in Concise Encyclopedia of Semiconducting Materials and Related Technologies, S.Makajah and L.C.Kimerling (eds.) (Pergamon, Oxford, 1992).
13. H.Temkin, T.P.Pearsall, J.C.Bean, R.A.Logan and S.Luryi: $Si_{1-x}Ge_x$ *strained layer superlattice waveguide photodetectors operating near 1.3*μ*m.* Appl. Phys. Lett. **49** (1986) 809.
14. D.J.Robbins, M.B.Stanaway, W.Y.Leong, J.L.Glasper and C.Pickering: $Si_{1-x}Ge_x$*/Si quantum well infrared photodetectors.* J. Mater. Sci.: Materials in Electronics **6** (1995) 363.
15. E.Kasper: *Prospects of SiGe heterodevices.* J. Cryst. Growth **150** (1995) 921.
16. C.Renard, S.Bodnar, P.A.Badoz and I.Sagues: *Tunable infrared photoemission sensor on silicon using SiGe/Si epitaxial heterostructures.* J. Cryst. Growth **157** (1995) 195.
17. E.Kasper and E.H.C.Parker (eds.): *Silicon molecular beam epitaxy 1995.* J. Cryst. Growth **157** (1995) nos. 1-4.
18. M.A.Herman: *Surfactants in heteroepitaxy of strained semiconductor structures.* Proc. SPIE **2373** (1995) 11.
19. T.Sakamoto, H.Funabashi, K.Ohta, T.Nakagawa, N.J.Kawai, T.Kojima and Y.Bando: *Well defined superlattice structures made by phase-locked epitaxy using RHEED intensity oscillations.* Superlattices and Microstructures **1**, 347-352 (1985).
20. V.A.Markov, O.P.Pchelyakov, L.V.Sokolov, S.I.Stenin and S.Stoyanov: *Molecular beam epitaxy with synchronization of nucleation.* Surface Sci. **250**, 229-234 (1991).
21. M.L.Larsson and G.V.Hansson: *Synchronization of nucleation studied with Monte Carlo simulations and applied to* $Si_{1-x}Ge_x$ *molecular beam epitaxy,* Surface Sci. **292**, 98-113 (1993).
22. M.Copel, M.C.Reuter, E.Kaxiras, R.M.Tromp: *Surfactants in epitaxial growth,* Phys. Rev. Lett. **63**, 632-635 (1989).
23. N.Usami, S.Fukatsu and Y.Shiraki: *Abrupt compositional transition in luminescent* $Si_{1-x}Ge_x$*/Si quantum well structures fabricated by segregant assisted growth using Sb adlayer.* Appl. Phys. Lett. **63**, 388-390 (1993).
24. R.A.Metzger: *Is silicon-germanium the new material for the future?* Compound Semicond. **1** (1995) no.3, 21.
25. P.Kruck, M.Helm, T.Fromherz, G.Bauer, J.N.Nützel and G.Abstreiter: *Medium-wavelength, normal incidence, p-type Si/SiGe quantum well infrared photodetector with background limited performance up to 85K.* Appl. Phys. Lett. **69** (1996) 3372.
26. G.Masini, L.Colace, F.Galluzzi, G.Assanto, T.P.Pearsall, H.Presting: *Voltage tunable SiGe photodetector: A novel tool for crypted optical communications through wavelength mixing.* Appl. Phys. Lett. **70** (1997) 3194.

